How to cite: *Angew. Chem. Int. Ed.* **2025**, e202516331
doi.org/10.1002/anie.202516331

Bioorthogonal Chemistry **Hot Paper**

Cyclometalated Gold(III)-Mediated Cysteine Arylation: A Bioorthogonal Platform for Covalent Targeting of Intrinsically Disordered Proteins

*Udara Munugoda, Sean T. Gilpatrick, Debarati Das, Sean Parkin, Anne-Frances Miller, and Samuel G. Awuah**

Abstract: Intrinsically disordered proteins (IDPs) remain largely inaccessible to covalent chemical tools due to their structural plasticity and lack of defined pockets. We introduce a bioorthogonal cyclometalated gold(III) platform of monodentate phosphine-supported AuP1-8 complexes that selectively and irreversibly arylate cysteine residues via enhanced *Lewis* acidity. This platform enables targeting of low-reactivity, buried, or dynamically disordered cysteines across the human proteome. Chemoproteomic, structural, and computational analyses establish an expanded ligandable cysteinome, including transiently helical LLCLL motifs in intrinsically disordered regions (IDRs). Our findings establish a new class of metal-mediated bioorthogonal reagents for proteome-wide cysteine labeling, functional interrogation of disordered proteins, and future therapeutic and diagnostic applications.

Introduction

Chemical tools that enable proteome-wide labeling of cysteines, particularly within intrinsically disordered regions (IDRs), remain scarce due to limitations in probe selectivity, hydrophobicity, and insufficient reactivity tuning. Whereas Au(III) complexes have emerged as promising scaffolds for bioconjugation[1–3] and their potential for global cysteine profiling across the human proteome, especially in the context of disordered or low-reactivity environments, remains largely unexplored. This study fills the gap with the design of novel bioorthogonal Au(III) scaffold compatible with click chemistry as a tunable, next-generation global cysteine profiling platform for drugging the undruggable proteins. Cysteine's nucleophilicity and moderate abundance in the proteome make it an attractive target for selective bioconjugation. A wide range of electrophilic reagents have been developed to engage cysteines under mild conditions with high chemoselectivity and tunable kinetics.[4–8] Fast cysteine bioconjugation typically refers to reactions with second-order rate constants (k_2) exceeding 10 M^{-1} s^{-1},[9,10] though commonly used reagents span a broad reactivity range (10^{-1}–10^5 M^{-1} s^{-1}), including alkyl halides, Michael acceptors, heteroaromatic nitriles, pyridinium salts, and maleimides (Figure 1).[9,11–17] Among these, maleimides offer relatively fast labeling ($k_2 \approx 10^2$ M^{-1} s^{-1}) yet suffer from hydrolysis and instability under physiological conditions.[9,11–18] Among these, maleimides offer relatively fast labeling ($k_2 \approx 10^2$ M^{-1} s^{-1}) yet suffer from hydrolysis and instability under physiological conditions.[13,17]

Despite recent innovations including activated heteroaromatics, hypervalent iodine, strain-promoted conjugation, and organometallic probes,[9,18–21] most bioconjugation chemistries still face key limitations including poor proteome-wide compatibility, reversibility, and limited access to buried or low-nucleophilicity cysteines. Furthermore, current profiling reagents preferentially label cysteines located in solvent-exposed, structured protein domains, leaving intrinsically disordered regions (IDRs) and loops underexplored. These disordered domains, characterized by conformational plasticity, often harbor cysteines that are transiently accessible, sterically shielded, or embedded in dynamic local environments.

To address this unmet need, we aimed to develop a class of highly reactive, biocompatible cysteine-targeting reagents that can label both conventional and structurally elusive residues across the proteome. Organometallic complexes, particularly those based on group 10 and 11 metals, have recently emerged as powerful tools for site-selective protein

[*] U. Munugoda, S. T. Gilpatrick, D. Das, S. Parkin, A.-F. Miller, S. G. Awuah
Department of Chemistry, University of Kentucky, Lexington, Kentucky 40506, USA
E-mail: awuah@uky.edu

S. G. Awuah
Center for Pharmaceutical Research and Innovation, Department of Pharmaceutical Sciences, College of Pharmacy, University of Kentucky, Lexington, Kentucky 40536, USA

S. G. Awuah
Markey NCI Comprehensive Cancer Center, University of Kentucky, Lexington, Kentucky 40536, USA

S. G. Awuah
University of Kentucky Bioelectronics and Nanomedicine Research Center, Lexington, Kentucky 40506, USA

D. Das
Present address: Department of Chemistry, University of Washington, Seattle WA 98195-1700, USA

Additional supporting information can be found online in the Supporting Information section

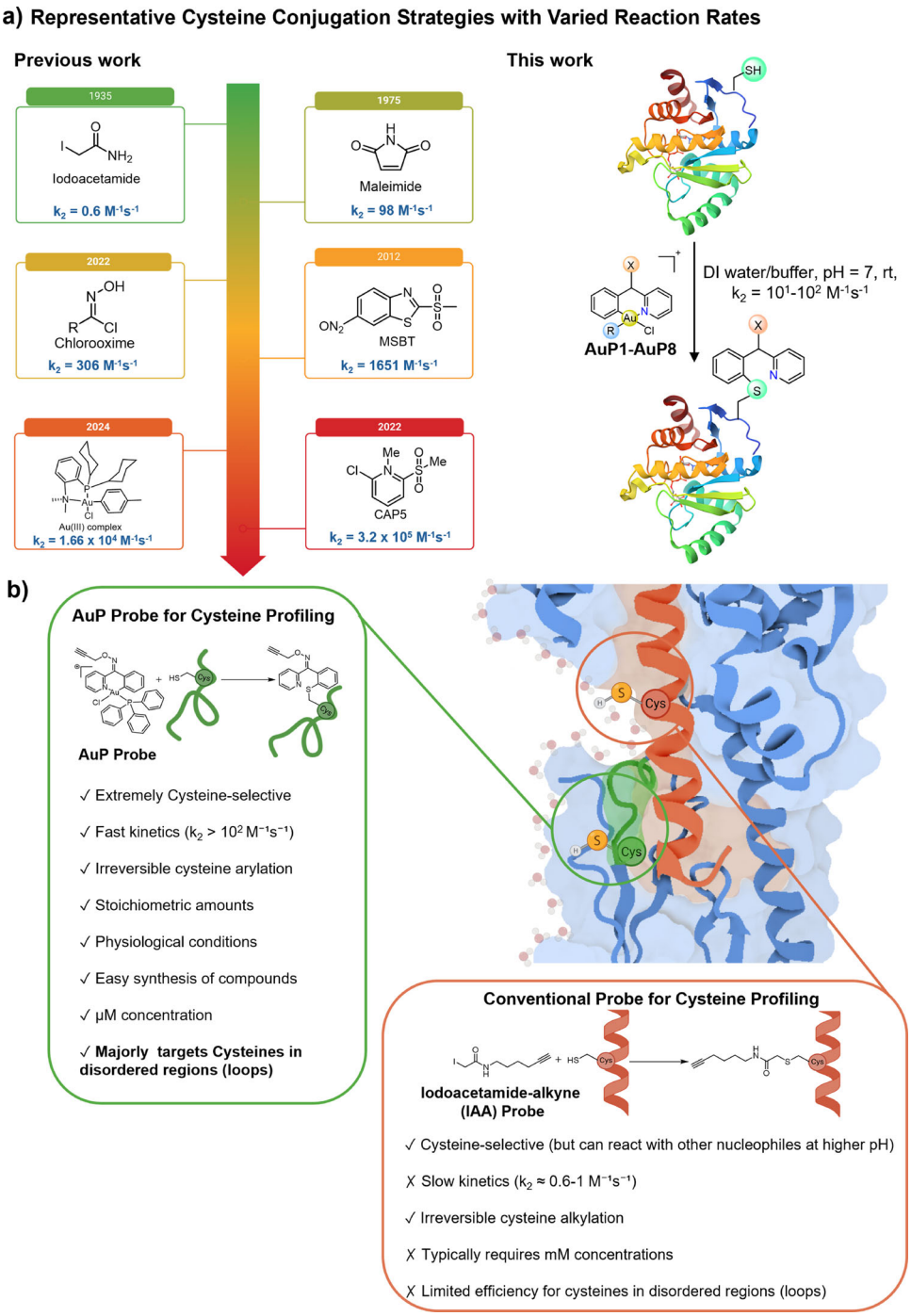

Figure 1. New monodentate phosphine [C^N]-cyclometalated Au(III) arylation reagents (**AuP**) as novel tools for Cys profiling and imaging. a) Comparison of second-order rate constants for cysteine bioconjugation, highlighting **AuP** reagents alongside standard organic electrophiles and representative bioorthogonal reactions. b) Visual representation of **AuP probe (AuP1-alkyne)**1 targeting nucleophilic cysteines, particularly those located in intrinsically disordered regions (IDRs) of proteins that are not accessible to traditional cysteine labeling reagents like Iodoacetamide-alkyne (**IAA**) probe accompanied bya schematic illustrating key properties of **AuP probe** compared to **IAA** demonstrates the arylation of a distinct subset of cysteines compared to traditional labeling probes: the combination of exceptional cysteine selectivity and the formation of stable and MS-detectable Cys adducts by **AuP probe** can be detected by both gel-based and MS-based chemoproteomic profiling in vitro.

modification, forming stable S–C(sp^2) and S–C(sp^3) linkages with high reaction rates under biologically relevant conditions.[21–25] Notably, cyclometalated palladium(II) and gold(III) complexes have been shown to enable aryl transfer to cysteine residues in biomolecules with exceptional chemoselectivity.[2,25–28] Gold-based reagents are especially attractive due to their favorable reactivity, biocompatibility, and tunable ligand frameworks.[29–31]

Our laboratory has previously leveraged gold complexes in protein labeling, catalysis, and drug discovery, including Au(I)-mediated lysine arylation of c-MYC and Au(III)-catalyzed cysteine modification of KRASˆG12C.[2,32–37] These studies, along with our development of metal-ligand affinity chemistry (MLAC), motivated the design of a next-generation class of cysteine-selective gold(III) arylating reagents.[34]

Covalent labeling probes provide foundational tools for target identification, drug discovery, imaging, and protein functional studies. Yet, despite advances in fragment-based discovery, the majority of human proteins remain undruggable, lacking selective ligands or modifiable residues.[38–42] Site-specific covalent labeling of endogenous cysteines without genetic modification presents an attractive strategy to engage these targets directly.[38–42] The integration of mass spectrometry with covalent modification has transformed proteomics, and electrophile tuning remains critical for expanding the accessible ligandable cysteinome.

Initial efforts to covalently engage proteins focused on catalytic cysteines within enzyme active sites (e.g., kinases, proteases), targeting nucleophilic residues such as cysteine, serine, and histidine.[43–45] Recent efforts have extended this strategy to noncatalytic functional residues, including in KRAS-G12C, the XPO1 substrate groove, and ATP-binding pockets of kinases, broadening the scope of covalent ligand discovery.[2,46–48] However, large swaths of the cysteine-containing proteome, including IDPs, PPIs, and glycan-binding proteins, remain largely unliganded and are considered functionally undruggable. Expanding chemical access to these proteins remains a key challenge.[49–53]

Herein, we report the synthesis and characterization of **AuP1-8**, a family of cyclometalated gold(III) complexes supported by monodentate phosphines, which function as both highly efficient cysteine bioconjugation reagents and proteome-wide labeling tools. These reagents display fast, irreversible S-arylation under physiological conditions, enabling high-coverage chemoproteomic profiling. AuP complexes preferentially label cysteines in solvent-accessible, flexible, and intrinsically disordered regions, including transiently reactive or partially buried sites overlooked by maleimide or iodoacetamide probes. In global proteome analyses, AuP reagents label internal (82.1%), C-terminal (17.7%), and N-terminal (0.2%) cysteines. Significantly, they also arylate cysteines within hydrophobic LxxLL motifs that stabilize residual helical structure in IDPs and support lipid-like environments amenable to covalent modification by lipophilic warheads. These reagents are air-stable, synthetically modular, and operate at low micromolar concentrations. Profiling reveals minimal overlap with conventional probes, enabling a new dimension of site-specific, gold-based protein labeling. Our results establish AuP reagents as a versatile and powerful new class of cysteine-directed bioconjugation tools. This approach opens the door to targeting elusive residues within the disordered proteome, expanding the frontier of covalent ligand discovery, target validation, and chemical biology.

Results and Discussion

Design, Synthesis, and Characterization of AuP Cysteine Arylation Reagents

We employed [CˆN]-cyclometalated Au(III) as the template for cysteine arylation (Figure 1a). The reactivity of the structural scaffold can be potentiated by tuning ancillary ligands. In our effort to fine-tune the cyclometalated scaffold for cysteine reactivity, we assessed the structure–activity profile across cycloaurated compounds with different monodentate phosphine ligands. Phosphine ligands are "soft" σ-donating compounds that enhance solubility and stability in organometallic complexes.[39,53] Through backbonding, these ligands donate their electron lone pair and accept electron density from metal d orbitals, influencing the reactivity of target metal complexes.[54] Cumulative evidence suggests that reductive elimination reactions in transition metal complexes are heavily influenced by the steric environment of bulky phosphine ligands around the metal centers.[55] Chemoselective arylation of biological nucleophiles occurs by either a mechanism-based transformation or reductive elimination, where the oxidation state of the metal center decreases while forming a new covalent C_{aryl}-X bond with the target biomolecule.[37,55–57] We synthesized a library of eight different cyclometalated Au(III) complexes with different monodentate phosphine ligands and assayed their reactivity and selectivity with cysteine using stopped-flow kinetics, mass spectrometry, and within the context of a complex proteome.

We investigated the impact of modifying phosphine ligands on the cyclometalated Au(III) [CˆN] framework, known for arylating the cysteine amino acid residue. After synthesizing the cyclometalated dichloridogold(III) [CˆN] compounds, we utilized ligand substitution methods to synthesize eight compounds bearing triphenylphosphine (PPh_3), 4-diphenylphosphino benzoic acid, Sphos, and Xphos phosphine ancillary ligands (Figure 2a). Single crystals of **AuP3–AuP7** were obtained by vapor diffusion of diethyl ether into dichloromethane solutions containing concentrated gold complexes, and their structural properties were determined by X-ray diffraction analysis. **AuP3–AuP7** maintain the square-planar geometry around the Au(III) center, confirmed by the X-ray crystallography (Figure 2b and see Figures S40–S44 and Tables S2–S6). **AuP1–AuP8** were characterized by ^{1}H, ^{31}P NMR spectroscopy, X-ray crystallography, and mass spectrometry, and the purity was established by HPLC > 95%. (See Figures S1–S39 and Tables S2–S6).

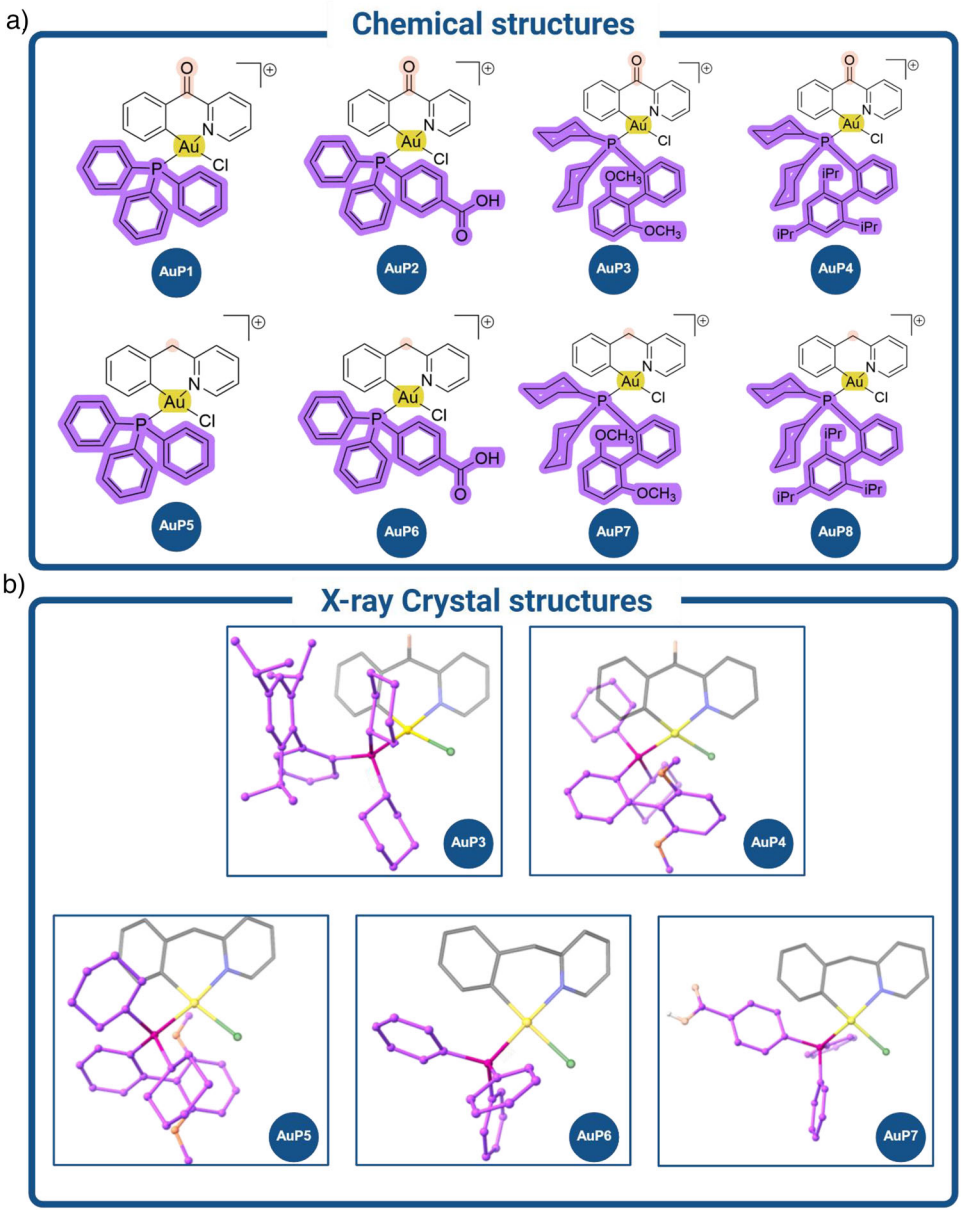

Figure 2. Chemical structures of complexes in this report. a) Chemical structures of novel monodentate phosphine [C^N]-cyclometalated Au(III) complexes (**AuP1–AuP8)** used in this study. b) X-ray crystal structures of **AuP3**–**AuP7**. Ellipsoids are drawn at 50%. Hydrogens, perchlorate anions, and solvent molecules have been omitted for clarity.

Cysteine Reactivity and Selectivity of AuP Reagents via Arylation

We initially examined biomolecule arylation by the gold-derived probe library to evaluate chemoselectivity versus relevant canonical nucleophilic amino acids at room temperature (Figures 3 and S45–S51). It was clear that rapid, full conversion of the arylated product occurred with only cysteine thiol. Reactions of the equimolar concentrations of gold-derived reagents with L-glutathione or N-acetyl cysteine (NAC) under mild conditions in 90:10 [H_2O]/[MeCN] at pH 7.4 showed quantitative conversion (> 99%) of arylated-L-GSH or arylated-NAC conjugates within 5 min, determined by LC-MS analysis of the crude reaction mixture (Figure 3a–e). We subsequently investigated the reactivity of other amino acids containing potential nucleophilic groups, including lysine (amine group), tyrosine (hydroxyl group), histidine (imidazole group), tryptophan (indole group), methionine (thioether group), and arginine (guanidino group). Notably, only cysteine (thiol group) formed a detectable conjugation product (arylated product) with Au(III)-monophosphine arylation (**AuP**) reagents, while the other amino acids did not (Figure 3f). This highlights the exceptional chemoselectivity of Au(III)-monophosphine arylation reagents for cysteine's thiol group over other nucleophilic sites in proteins.

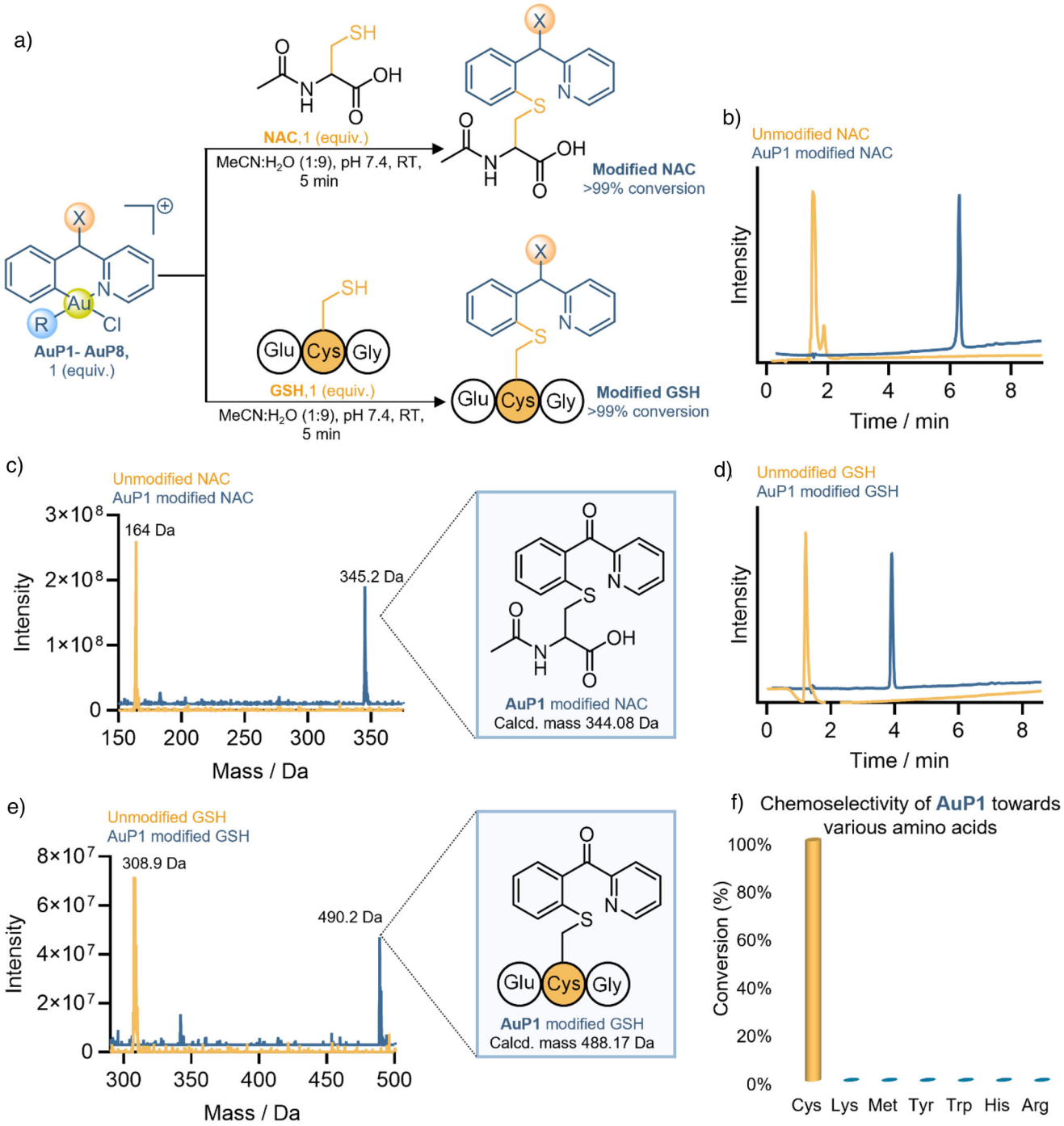

Figure 3. Chemoselectivity of **AuP** reagents by arylation. a) Chemoselective cysteine arylation by **AuP1–AuP8** of N-acetyl cysteine (NAC) and tripeptide; glutathione (GSH). Reaction conditions: Probe **AuP1–AuP8** 6 mM with NAC 6 mM at pH 7.4, room temperature after 5 min, probe **AuP1–AuP8** 3.2 mM with GSH 3.2 mM at pH 7.4, room temperature after 5 min. b) and c) An example of LC chromatogram and LC-MS spectrum showing the cysteine arylated product of NAC + **AuP1**. d) and e) LC chromatogram and LC-MS spectrum showing the cysteine arylated product of glutathione GSH (3.2 mM) cysteine arylation by AuP1 (3.2 mM) at pH 7.4, room temperature, after 5 min. f) Conversion % of different amino acids by **AuP1**.

To demonstrate site-specific modification, we used bovine serum albumin, which has eight disulfide bonds and one free thiol. Specifically, we showed that these complexes selectively target only the free cysteine thiol without disrupting the cysteine disulfide bonds in proteins. **AuP1** and **AuP7** (40 μM) were incubated with BSA (8 μM) at room temperature in 90:10 [H_2O]/[MeCN] at pH 7.4 (protein/Au(III) complex = 1:5) (Figure 4a). The labeled protein was then analyzed using tandem LC-MS/MS after digestion with trypsin. This revealed covalent modification of BSA at C34 by probe **AuP1** or **AuP7** in a manner consistent with C–S arylation, as indicated by the MS result of $m/z = 167$ and 180 (Figure 4b,c).

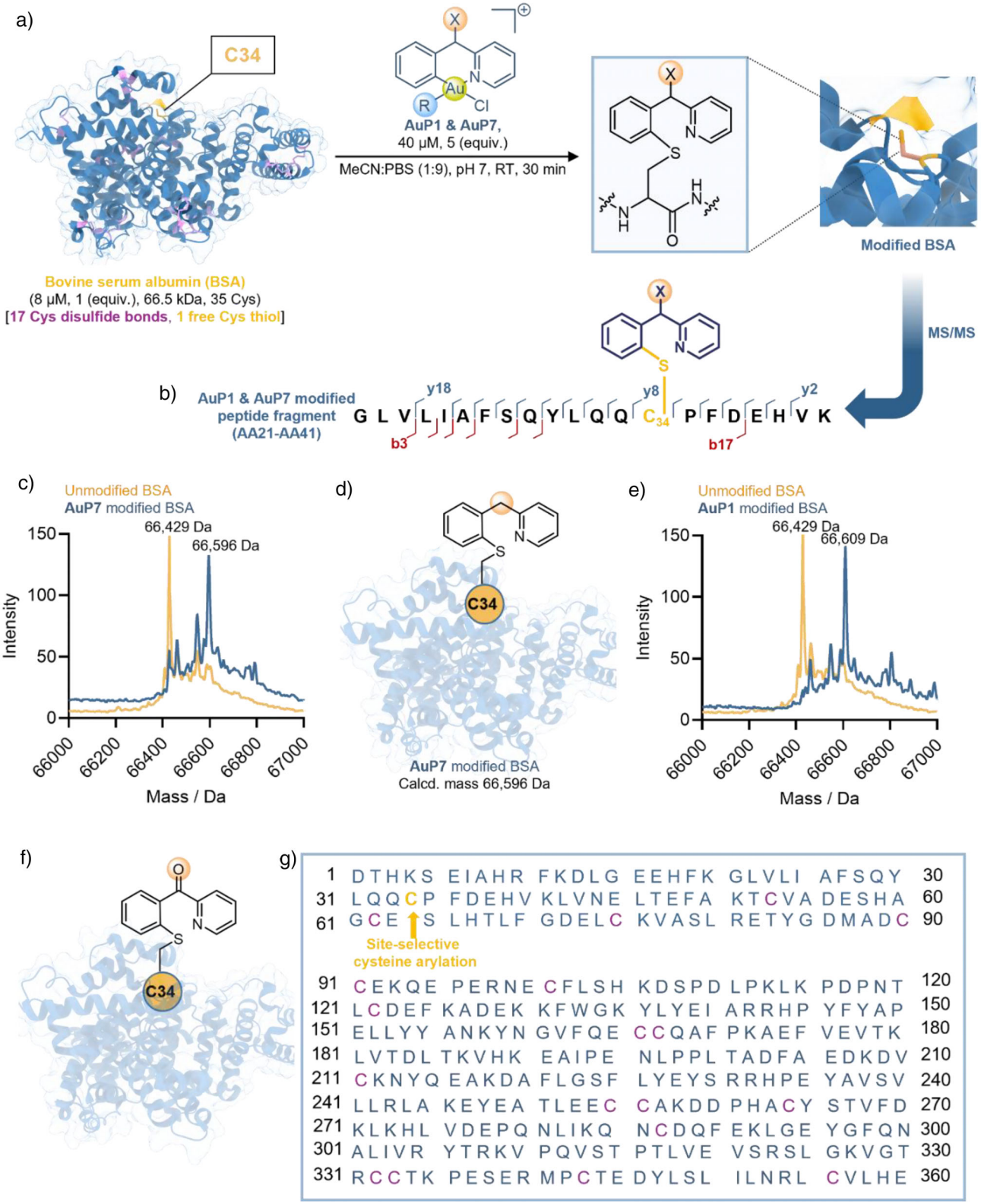

Figure 4. Chemoselective Au(III)-mediated arylation of protein. a) Extreme cysteine thiol-specific labeling of BSA protein by **AuP1 & AuP7**, the only modified free thiol of Cys34 residue is highlighted in yellow. Intact mass analysis: Deconvoluted LC/MS spectrum demonstrating covalent modification of BSA by **AuP1** and **AuP7**. The free thiol of Cys34 (highlighted in yellow) undergoes selective bioconjugation, as confirmed by intact mass analysis. b) the tryptic peptide formed containing residues 21–41 from BSA-AuP1, confirming Cys34 modification. c) ESI-MS spectra of unmodified BSA (observed mass: 66,596 Da) and BSA treated with **AuP7** (calculated: 66,596 Da; observed: 66609.03 Da). d) Model of product formed by reaction of **AuP7** with BSA. e) ESI-MS spectra of BSA-**AuP1** (calculated: 66,611 Da; observed: 66609.03 Da), showing a mass shift consistent with site-specific **AuP1** adduct formation. f) Model of product formed by reaction of **AuP1** with BSA. g) Sequence showing site-selective cysteine arylation.

No other tryptic peptides were modified, confirming specific arylation only at C34, the one cysteine with a free thiol group in BSA (Figure 4b,c). No modifications were observed at the other 16 oxidized cysteine residues that formed disulfide bonds in the protein. This indicates the chemoselectivity and regioselectivity of Au(III) complexes towards the free thiol groups in cysteine residues.

Under pseudo-first-order conditions, stopped-flow experiments were conducted with GSH and **AuP4** and **AuP5**, which contain bulkier groups. While we anticipated the detection of the cysteine-ligated construct, an intermediate we had previously characterized by X-ray crystallography,[2] its extremely rapid consumption precluded detection in this experimental setup. Also, due to the rapid nature of this reaction, the dsappearance of the absorbance of **AuP4** and **AuP5** could not be monitored. Consequently, the appearance of the absorbance of the cysteine-arylated product at 260 nm was measured, revealing second-order rate constants for the reaction of **AuP4** and **AuP5** under pseudo-first-order conditions (GSH as 8.2×10^1 and $1.23 \times 10^2\ M^{-1}s^{-1}$, respectively (see Figure S52 and Tables S7–S9). Similarly, we calculated rate constants for cysteine arylation of NAC with **AuP4** and **AuP5**, resulting in values of 0.58×10^2 and $0.9 \times 10^2\ M^{-1}s^{-1}$, respectively (see Figure S52 and Tables S7, S10, and S11). Analyzing the kinetic data revealed that **AuP4** and **AuP5** react more rapidly with GSH than with NAC. The stopped-flow traces are best described by a two-step model: (1) a very fast pre-equilibrium coordination of the cysteine thiol to the Au(III) center (bioconjugation step), followed by (2) reductive elimination to form the Au–S arylated product (arylation step). The initial coordination is so fast that it cannot be directly resolved or monitored by stopped flow apparatus, but its equilibrium constant and apparent rate (k_{co}) still influence the effective k_{obs} values. Therefore, these significant non-zero intercepts reflect this fast pre-equilibrium thiol coordination, which could be a zero-order pathway. This discrepancy can be attributed to the stronger reducing capacity of GSH compared to NAC, stemming from its more negative reduction potential of (−240 mV) at higher concentrations around 1–13 mM.[58] It should be noted that the use of a more sterically hindered phosphine ligand, such as Xphos, with the C^N cyclometalated Au(III) framework; **AuP4** resulted in a slower rate of cysteine arylation compared to the less sterically hindered phosphine ligand, PPh_3, with the Au(III) framework; **AuP5**. The electronic characteristics of the phosphine ligands and the structural features of ketone ($C^{CO}N$) versus methylene bridges ($C^{CH2}N$) of the cyclometalated C^N complexes impact reactivity and rates. For example, carbonyl bridge is more electron-withdrawing than a methylene bridge, conferring electrophilicity at the gold center. We considered Tolman Electronic Parameter (TEP) values as a qualitative guide. In general, more electron-rich (strong σ-donor) phosphines tend to push electron density toward the Au(III) center, which could slightly reduce the complex's electrophilicity and potentially slow down the cysteine arylation rate. Taken together, opportunities to confer site selectivity by these reagents exist, which prompted an investigation into the steric profiles of phosphine ligands on the Au(III) metal center.

Theoretical Analysis of Ligand Effect on Cysteine Arylation

To gain insights into the influence of phosphine ligands on cysteine arylation, we analyzed the steric environment around the Au(III) center using percent buried volume (V_{Bur}%) calculations. This metric quantifies how much of the coordination sphere around the metal is occupied by the ligand, showing how a bulky ligand can hinder an incoming thiol's access to the metal center and thereby influence the reaction rate.[59] We analyzed their steric profiles via percent buried volume (V_{Bur}%) calculations using the SambVca 2.1 web application,[60] with the other **AuP** complexes as well. (Figures 5 and S53–S60).

For optimized structures, all calculations were performed using the Gaussian 16 (Rev. A.03) software package.[61] Ground-state geometries of the investigated structures were optimized in water using the CPCM implicit solvation model[62] with density functional theory (DFT) using the ωB97X-D exchange–correlation functional[63] with the def2-TZVP basis set for all atoms.[64,65] Initial structures were extracted from experimental X-ray crystallographic data when available or created manually in cases where no crystal structure existed. Optimization and frequency calculations were performed at the same level of theory, and no imaginary frequencies were detected, confirming that all optimized structures correspond to true minimum.

The more sterically hindered **AuP4** showed a slower rate constant experimentally (Figure S52 and Table S7) and has a $\%V_{Bur}$ value of 67.5, whereas the less hindered **AuP5**, with a higher rate constant, has a $\%V_{Bur}$ value of 65.7 (Figure 5d,e).

This correlation suggests that increased steric bulkiness around the metal center can reduce the reaction rate, potentially by hindering the departure of the leaving group. However, given the limited number of **AuP** complexes examined, these observations remain preliminary, and additional data are needed to verify whether this is a generalizable trend for this system. Nonetheless, the initial findings present the possibility of tuning the reactivity profile of the metal center via its phosphine ligand to control the reactivity toward cysteines. As previously explained, combining the effect of cyclometalation with less bulky phosphine ligands can accelerate the cysteine reactivity. A clear example of that is the 2-benzoylpyridine ($C^{CO}N$) cyclometalated Au(III) complex, which is more prone to reductive elimination with the smaller triphenylphosphine (PPh_3) ligand, **AuP1**. In our kinetic experiments, **AuP1** reacted with cysteine so rapidly that neither the bioconjugation nor the arylation step could be measured within the stopped-flow timescale used.

Target Profiling in Cells

Motivated by the rapid chemoselective Au(III)-mediated cysteine arylation capability of these complexes in model peptides and proteins, we aimed to assess protein targets in a cellular context by chemoproteomics and globally map its proteomic interactions. We modified **AuP1** with a terminal alkyne group (**AuP1-alkyne**), enabling selective protein labeling and enrichment via CuAAC-mediated click chemistry (Figure 6a).

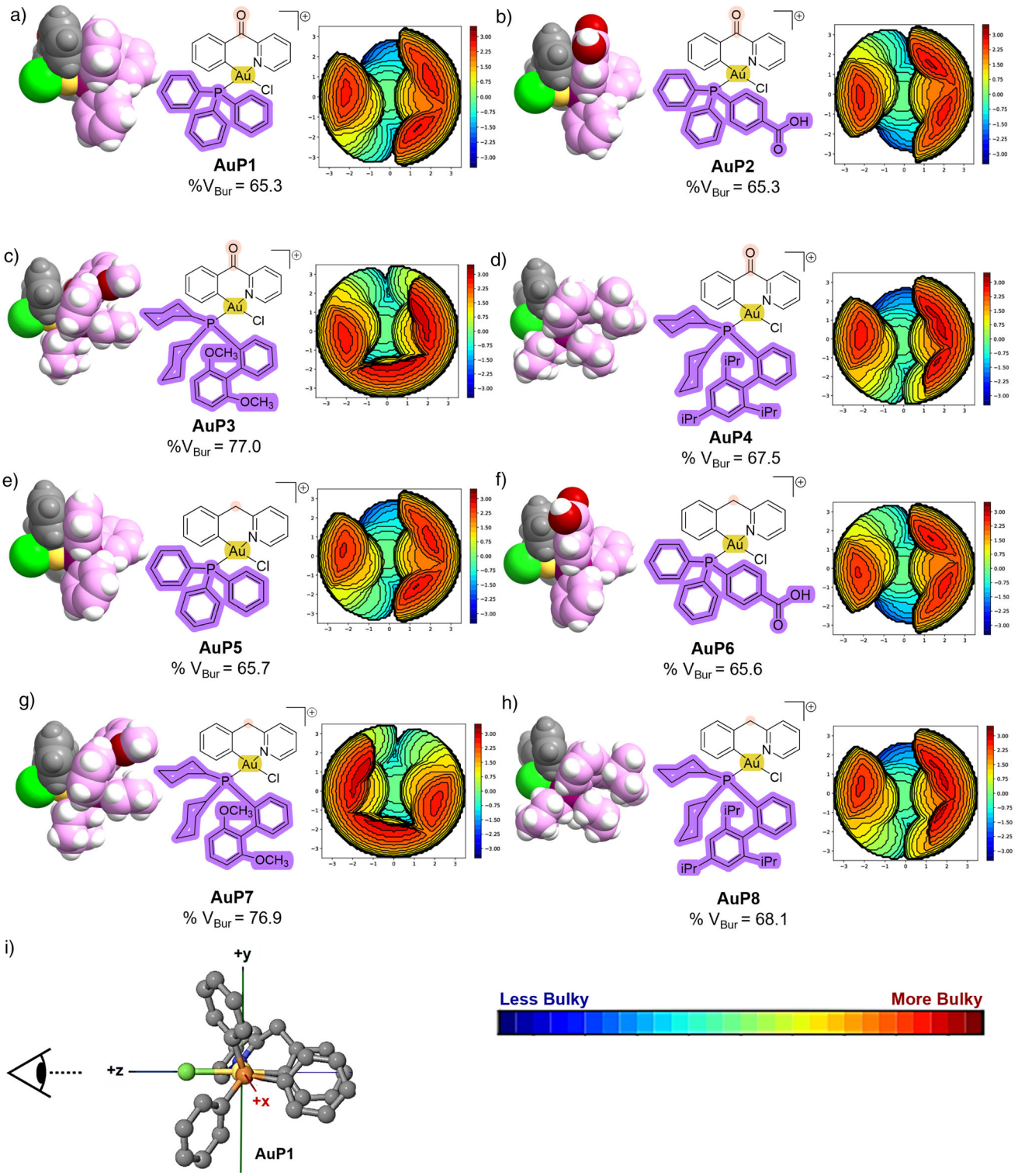

Figure 5. Computational analysis of ligand effect. a–h) $\%V_{Bur}$ analysis of **AuP1-AuP8** showing the steric maps produced by different ligands. Each is centered on the Au atom and shows the extent to which it is enclosed by ligand or accessible from solvent. The Z axis is aligned on the Au–Cl bond, the view is from Cl atom toward Au, the plane of view contains the Au atom, and the Au—Cl bond is in the XZ plane in the positive X direction. The field of view has a radius of 3.5 Å. i) Viewing orientation of the **AuP1** complex along the Au—Cl bond with defined x, y, and z axes for buried volume analysis.

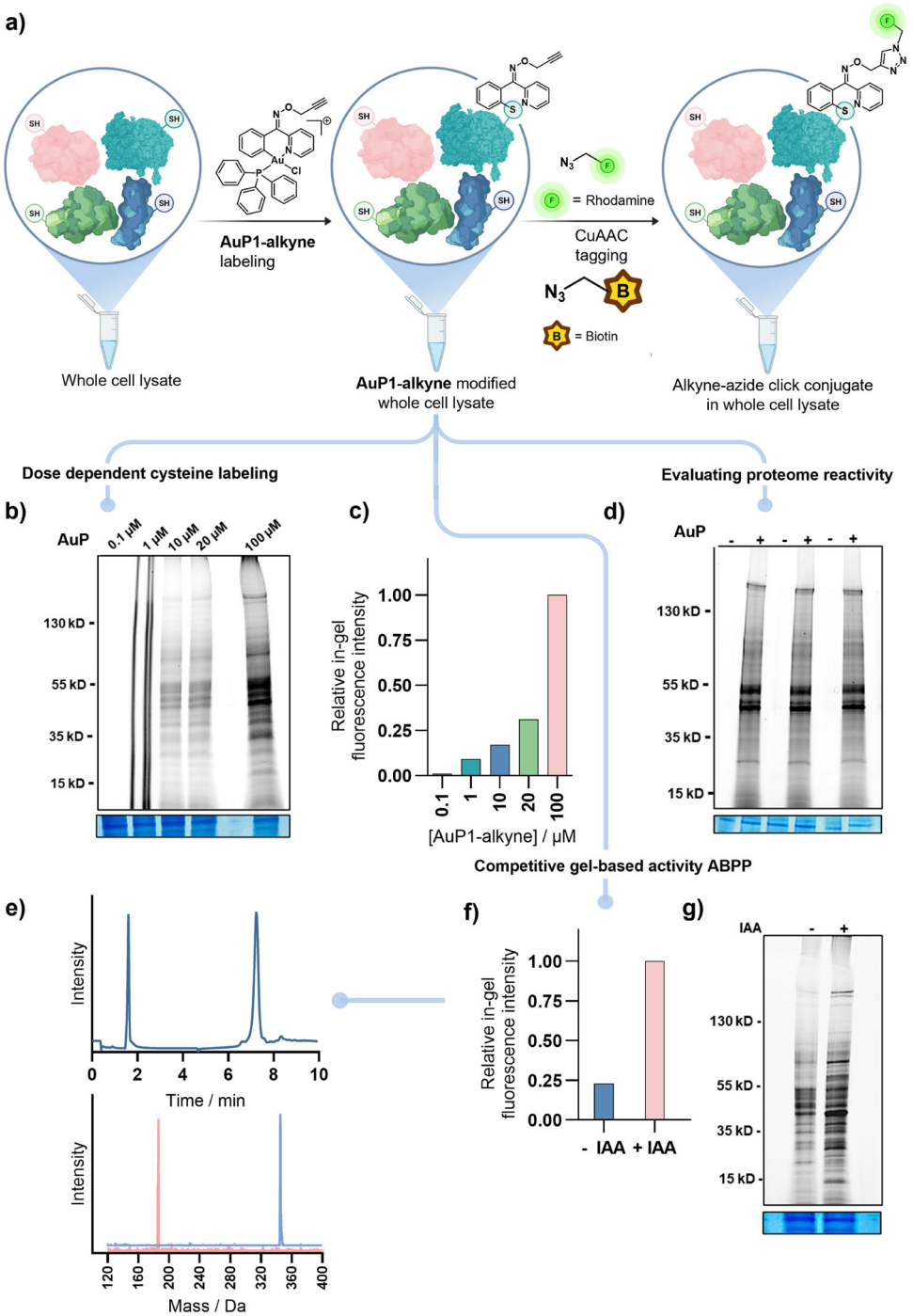

Figure 6. Gel-based proteome reactivity of **AuP1-alkyne** shows highly efficient Cys labeling in cell lysates. a) Schematic illustration of the whole proteome labeling by **AuP1-alkyne** followed by Rhodamine and biotin azide enrichment via CuAAC bioorthogonal reaction used in this study. b) Dose-dependent in-gel fluorescent cysteine labeling. Main panel is visualized by rhodamine fluorescence, whereas the panel below shows total protein as revealed by Coomassie brilliant blue as a reference. c) Quantification of in-gel labeling by **AuP-alkyne** extracted from (b). d) Evaluating proteome reactivity of **AuP1-alkyne** at 20 µM. e) Top LC and bottom MS of iodoacetamide competition with **AuP1** in the presence of NAC, showing that IAA does not modify NAC in the presence of **AuP1**. f) and g) Competitive gel-based activity ABPP with relative intensities derived from iodoacetamide (IAA) competition with **AuP1-alkyne**.

This modification allowed for protein reactivity analysis using in-gel fluorescence or biotin affinity tag with subsequent mass spectrometry analysis. The experiments utilized the proteome of the MDA-MB-231 human breast cancer cell line, an adherent epithelial cell line exhibiting a complementary protein profile.[66] MDA-MB-231 cells were subjected to **AuP1-alkyne** labeling, where cell lysates were incubated with the probe in a dose-dependent manner with 0.1, 1, 10, 20, and 100 μM for 1 h (Figure 6b and Table S12). This was followed by CuAAC-mediated conjugation with rhodamine-azide (Rh-N_3) and SDS-PAGE separation. As shown in Figure 6b–d, labeling at 100 μM revealed prominent bands for further competition studies with iodoacetamide. In-gel fluorescence imaging revealed prominent protein bands at 15, 20, 50, and 55 kDa (Figure 6d), indicating binding of the probe to proteins in these molecular weight ranges. These bands stood out prominently in the sample treated with 100 μM **AuP1-alkyne** but were not stronger than others when total protein was visualized by staining with Coomassie brilliant blue (Figure 6b). Overall, we demonstrated performance in gel-based activity-based protein profiling (ABPP) experiments via three different approaches: (1) single-concentration probe labeling to assess general cysteine reactivity, (2) dose-dependent ABPP to evaluate labeling across a range of probe concentrations, and (3) competitive ABPP (Figure 6b,d), in which lysates were pretreated with iodoacetamide prior to probe labeling to determine cysteine selectivity. Labeled proteins were separated by SDS-PAGE and visualized by fluorescence imaging.

Our probes also enable MS-based chemoproteomics for comprehensive profiling of cysteine reactivity and ligand engagement across the proteome. In this study, MDA-MB-231 cell lysates were treated with the **AuP1-alkyne** probe to investigate gold(III)-mediated cysteine arylation by bead-based biotin-streptavidin pulldown. Following probe treatment, cysteine-containing peptides were enriched and analyzed by mass spectrometry, allowing for the identification and quantification of probe-modified cysteine sites. This label-free, high-throughput approach provides robust coverage and reproducibility, revealing both conserved and previously uncharacterized cysteine residues targeted by **AuP1-alkyne** in the cellular context. Such profiling advances our understanding of gold-based covalent modification in complex proteomes and highlights new opportunities for targeting functionally relevant cysteines in cancer cells.

Our MS-based chemoproteomic approach, which relies on direct labeling and positive enrichment of probe-modified cysteines, provides greater accuracy than traditional activity-based probe profiling (ABPP) methods that infer binding by loss of signal.[67] ABPP suffers the risk of false positives due to compound-induced changes in proximal post-translational modifications (PTMs), redox state, or protein conformation, all of which can affect cysteine accessibility or arise from sample handling artifacts.[67] By contrast, our method directly tags and enriches probe-bound cysteines, minimizing these confounding factors and improving target identification fidelity. Nevertheless, we acknowledge that accessibility analysis itself has limitations, such as the inability to fully account for dynamic protein conformational changes or transiently exposed cysteine residues.

Au(III)-Mediated Click Chemistry for Chemoproteomic Profiling in Cells

We report the first successful use of a gold probe for unbiased cysteine labeling in human cell lysates via a one-pot CuAAC workflow (Figure 6a). Despite prior concerns that gold complexes may undergo side reactions with copper or fail in complex proteomes, our approach enabled robust biotin tagging and enrichment of a broad set of proteins under mild conditions. This demonstrates that Au(III) arylating reagents, previously applied only to purified proteins, can function as effective bioconjugation tools in proteomic settings. The workflow aligns with parameters used in public chemoproteomic datasets, facilitating integration and comparative analysis. Importantly, direct labeling via the **AuP1-alkyne** circumvents limitations of competition-based ABPP profiling and provides high-confidence enrichment of ligandable cysteines. These findings establish Au(III) complexes as a viable platform for global cysteine profiling and chemoselective protein conjugation.

A total of 3487 proteins were identified in the pull-down experiment using whole cell lysate from MDA-MB-231 cells (Figure 7a,c). The resulting protein profiles showed a remarkable diversity of cysteine targeting across the cancer cell proteome. To rigorously validate **AuP1**-biotinylation of cysteine-containing peptides, we implemented a targeted mass spectrometry workflow. Initially, LC-MS/MS data were searched for peptides bearing the precise mass of the **AuP1-biotin** modification using Byonic software, enabling selective identification of modified species (Figure 7b).

To fully understand the potential utility of the Au-based arylation reagents developed, we deemed it necessary to determine if proteins found in our data set have been identified and modified by previously published cysteine-modifying warheads. Our analysis revealed that ligandable cysteines are enriched in intrinsically disordered regions (IDRs) and exhibit intermediate burial, positioned 4–6 Å from bulk solvent with coordination numbers of 30–40 (Figure 7d–f). Over 50% of proteins harboring these cysteines lacked structured regions in their resolved PDB structures, consistent with their IDR-dominated conformations. These cysteines reside in hydrophobic microenvironments, often flanked by basic residues (e.g., lysine, arginine) that modulate local thiol pKa. Structural proximity analysis within a 6 Å radius further identified amino acid neighbors associated with ligandability in specific protein families, underscoring the importance of tertiary structure over primary sequence in determining cysteine reactivity. This is further confirmed by sequence logo analysis, a graphical representation that displays amino acid conservation and frequency at each position around modified cysteines. **AuP1-alkyne**-modified cysteines align with the well-characterized "LxxLL" leucine motifs that stabilize residual helical structure in intrinsically disordered proteins and create lipid-like microenvironments conducive to lipophilic warheads (Figure 7k). The "LLCLL" targeting strategy imparted

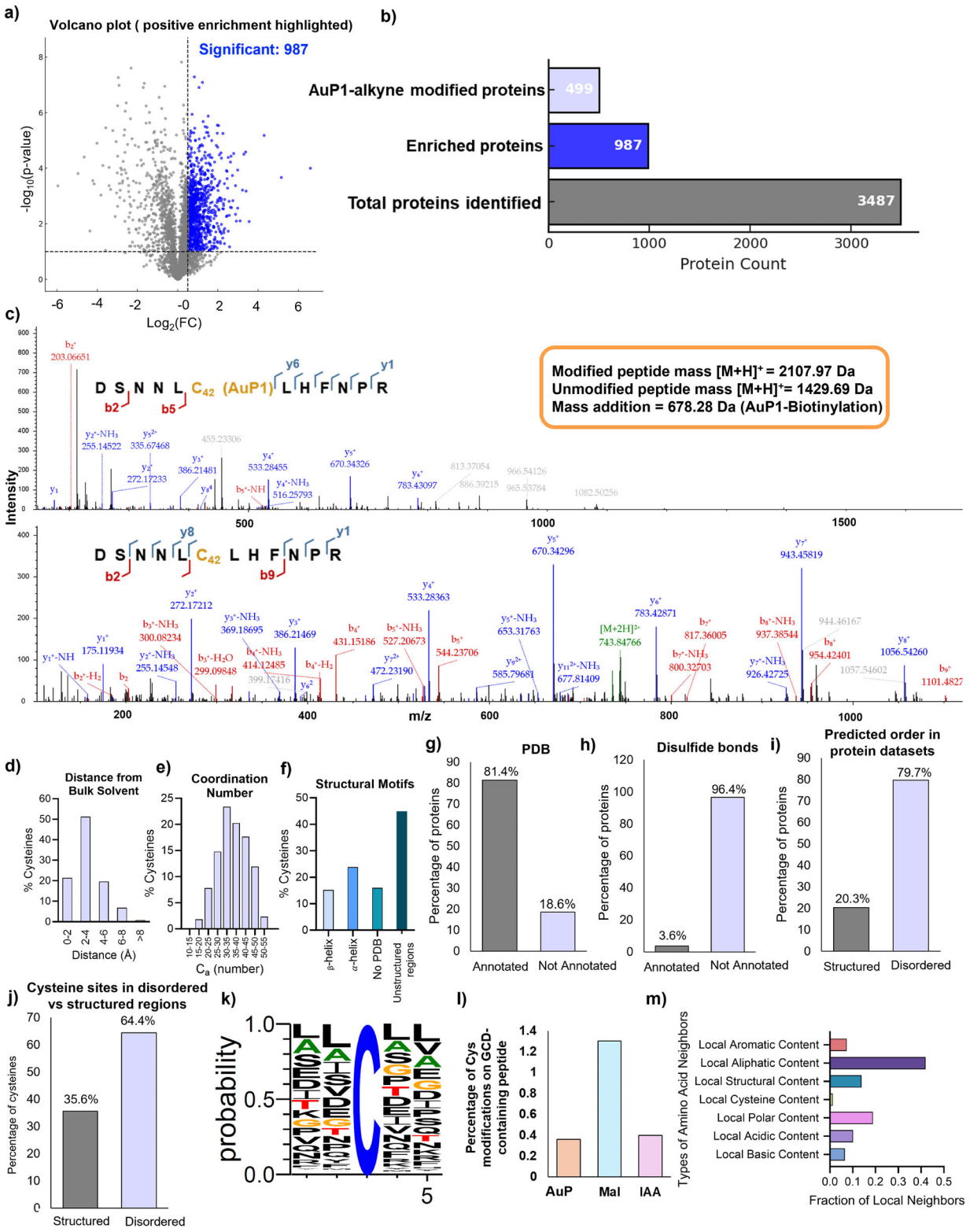

Figure 7. Chemoproteomic profiling of **AuP1-alkyne** in cells and comparative analysis with cysteine databases. a) Volcanic plot showing 987 significant proteins from a total of 3487 proteins. b) Bar chart showing total, enriched, and **AuP1-alkyne**-modified proteins. c) Selected MS/MS analysis showing peptide modification of cysteine by **biotinylated-AuP1** (*m/z* 678.28 Da) in galectin 1 from the whole proteome along with control. d) and e) Structural analysis of cysteines modified by biotinylated **AuP1-alkyne**. f) Structural motif of targeted cysteines by **AuP1-alkyne** in proteins showing predominant unstructured protein domains. g) Percentage of **AuP1-alkyne** modified proteins within the protein data bank (PDB) shows 18.6% of proteins not annotated. h) Analysis of disulfide bond-containing proteins modified by **AuP1-alkyne**. i) Intrinsically disordered protein prediction. j) Intrinsically disordered region prediction. k) Sequence logo map of **AuP1-alkyne**-modified cysteines. l) Cys modification on GCD-containing peptide. m) Neighboring amino acids of **AuP1-alkyne** modified cysteines.

by **AuP1-alkyne** not only fosters hydrophobic compatibility but also enables proximity-driven reactivity and optimal warhead positioning at protein sites. A striking example is seen in galectin-1 (vide infra), where Cys42 emerges as the dominant **AuP1** modification site exhibiting the highest spectral abundance and confidence scores, demonstrating the practical utility of targeting LLCLL-containing cysteines in complex proteomes. Further, the **AuP1-alkyne** probe has a lower preference for labeling cysteines within GCD motifs compared to both maleimide and IAA. (Figure 7l **AuP1**: 0.36%, Maleimide: 1.3%, IAA: 0.4%). This reduced reactivity extends to the tripeptide glutathione (GSH; γ-ECG), which shares the GCD sequence in its core structure. The lower interaction with GCD-containing sequences can explain the significantly lower reactivity of **AuP1** toward antioxidants like GSH, a critical advantage in biological contexts where GSH is abundant (~1–10 mM intracellularly) and competes with cysteines in proteins for labeling. This can reduce off-target effects.

Mechanistically, our extensive structural analysis of **AuP1-alkyne** targeted proteins suggests that its bulky C^N ligand and lipophilic PPh_3 groups create a steric shield around the Au(III) center, preventing engagement with solvent-accessible cysteines packed tightly in the structured regions in proteins. (Figure 7f–j). The hydrophobicity of the PPh_3 ligand (logP $\approx$ 4.2) in **AuP1-alkyne** enables membrane penetration and drives selectivity towards lipophilic regions, such as transient cavities and deeply buried cysteines in tightly packed cores (e.g., zinc finger domains), which remain inaccessible for most of the conventional cysteine probes. Unlike most of the probes, which favor solvent-accessible cysteines in structured regions, our **AuP** reagents target dynamic, disordered regions with intermediate burial (Figure 7f–m). This selectivity is critical for profiling cysteines involved in allosteric regulation or protein-protein interactions, which are underrepresented in existing structural databases.

To evaluate **AuP1**'s unique labeling patterns of proteins, we compared its targets to major cysteine-reactive probe datasets (CysDB, DBIA, NAIA-5, DrugMap). **AuP1** uniquely labeled 155 cysteines and 18 proteins not captured by any other probe and showed minimal overlap (only 29 proteins) across 499 labeled proteins compared to CysDB, DrugBank, ChEMBL, and FDA targets (Figure 8e, g). These results underscore **AuP1's** ability to access a distinct set of cysteines untargeted by conventional warheads, supporting its potential as a novel covalent drug scaffold (Figure 8a–c).

Importantly, thioredoxin-family proteins, including thioredoxin reductase, lack buried cysteines and instead present highly reactive, surface-exposed cysteine or selenocysteine residues. These sites are well-established targets for Au(I) complexes such as auranofin and cyclometalated Au(III)-choro ligands via selenol coordination.[68] However, the steric and electronic properties of our **AuP1** appear to limit such nonspecific interactions. This selectivity was supported by our multi-omics analysis of Pfam domain enrichment, which notably did not identify any thioredoxin or redoxin-family domains among the top 20 enrichments (Figure 8k). These domains are typically among the most highly represented in cysteine-reactive profiling studies. Our data confirm that **AuP1** labeling selectively avoids these canonical off-targets. This indicates that the structural design of **AuP1** contributes to enhanced selectivity by excluding common thiol-rich redox-active proteins.

To investigate the functional relevance of proteins labeled by **AuP1**, we employed a multi-omic data integration approach. By combining chemoproteomic data with genomic and structural annotations, we aimed to understand the functional roles of chemoproteomic-detected amino acids and identify therapeutically relevant sites. The functional enrichment analysis of **AuP1** modified proteins reveals a distinctive selectivity profile that sets it apart from conventional cysteine-reactive probes such as iodoacetamide and acrylamides (Figure 8). Unlike these conventional electrophiles, which predominantly target catalytic or hyperreactive cysteines in redox enzymes (e.g., thioredoxins, dehydrogenases), **AuP1** preferentially labels proteins associated with macromolecular complexes, membrane organization, and RNA metabolism (Figures 8f and S69). Notably, pathway analysis (Figure 8c) highlights significant enrichment in CORUM complexes and human phenotype-linked proteins, rather than canonical enzymatic pathways. Protein family analysis (Figure 8b) identifies chaperonins (TCP-1 complex), annexins, heat shock proteins, and mitochondrial carriers among the top enriched families, which are generally underrepresented in datasets from traditional probes. Subcellular localization data (Figures 8f and S69d) further show a strong bias toward peripheral and integral membrane proteins, cytoplasmic compartments, and organelle membranes, suggesting that **AuP1** effectively accesses surface-exposed cysteines in disordered or loop regions. GO biological process and molecular function enrichment (Figure 8d) reveals a strong association with cytoplasmic translation, ribosome biogenesis, RNA binding, and ATP-dependent activities, again distinguishing **AuP1-alkyne**-labeled proteins from the most common protein enzymes of conventional warheads. Finally, domain-level classification (Figure S69a,b) shows enrichment of Pfam families related to RNA recognition, WD40 repeats, DEAD box helicases, and other nucleic acid-associated proteins. Collectively, these results underscore the unique capability of the Au(III)-phosphine probe to map cysteines in structurally and functionally distinct protein classes, particularly those within intrinsically disordered regions, RNA-binding interfaces, and membrane-associated domains sites that are typically not targeted by conventional cysteine-reactive warheads. Standard electrophilic probes often display redundant reactivity profiles, primarily due to shared design constraints inherent to organic warheads, such as limited tunability, poor access to disordered or hydrophobic regions, and competition from abundant nucleophiles like glutathione. In contrast, the distinct steric and electronic properties of the **AuP** probes enable them to access these underexplored cysteine environments with high selectivity. Its structural design also offers the potential for further optimization, allowing rational tuning of reactivity toward specific cysteine subtypes based on structural context or proteome-wide reactivity to expand the ligandable proteome.

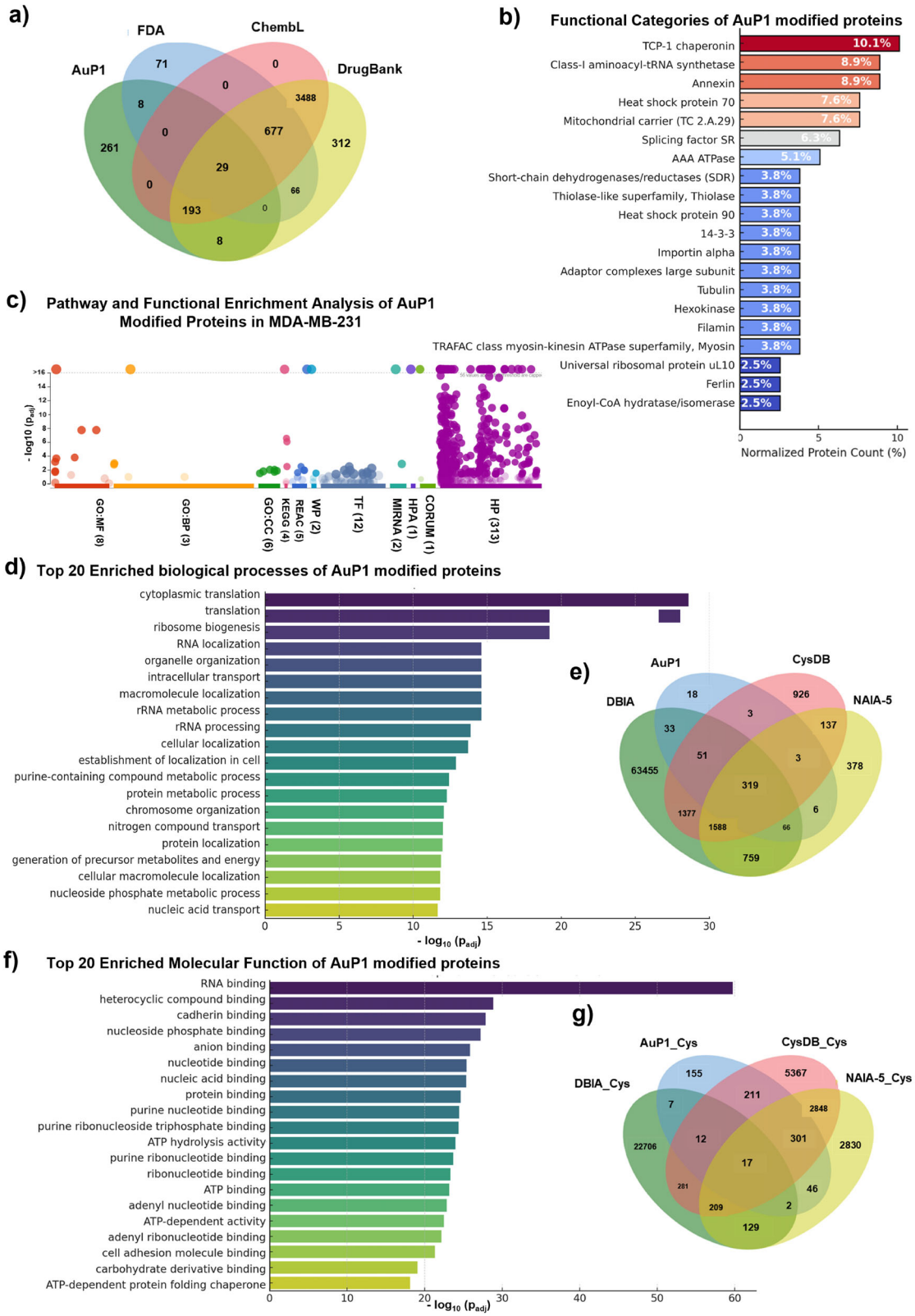

Figure 8. Multi-omic analysis of **AuP1 (AuP1-alkyne)** cysteine profiling data. a) Overlap between **AuP1**-targeted proteins and the proteins targeted by FDA-approved drugs and small molecules in DrugBank and ChEMBL. b) Functional categories among **AuP1**-targeted proteins. c) Functional annotation clustering of **AuP1-alkyne**-labeled proteins using g:Profiler. d) Top 20 enriched clusters of biological processes (BP) from GO-term analysis of **AuP1**-targeted proteins. e) Multiple comparison Venn diagram for AuP1 targeted proteins overlapping with cysteine profiling databases: CysDB, DBIA, and NAIA-5. f) Top 20 enriched clusters of molecular function (MF) from GO-term analysis of **AuP1**-targeted proteins. g) Multiple comparison Venn diagram for **AuP1** targeted cysteines overlaps with cysteine profiling databases: CysDB, DBIA, and NAIA-5.

Validation of Protein Targets Engaged by Probe in Cells

To confirm preferential probe-protein interactions identified in target profiling, galectin-1 (LGALS1) was chosen because of its association with the immune response and its sensitivity to redox status via reduction/oxidation of its Cys side chains. Galectin-1 is a small protein (14.7 kDa, 135 amino acids) often found in increased amounts in malignant cancers.[69] It possesses six cysteine residues (Cys2, Cys16, Cys42, Cys60, Cys88, and Cys130). In its extracellular state, galectin-1 is typically in a reduced form, containing six free thiols.[70] However, oxidants, commonly present in various pathological processes, convert thiol groups to disulfides, adding a dynamic dimension to galectin-1′s behavior that may provide a signal for pathological conditions.

To test for the site-specific modification of galectin-1, we incubated **AuP1** (86.2 μM) with recombinant galectin-1 (17.2 μM) at room temperature in phosphate buffered saline (PBS) at pH 7.4 (protein/**AuP1** = 1:5) (Figure 9b). The labeled protein was then analyzed using tandem LC-MS/MS, showing that **AuP1** modified all six cysteine residues in galectin-1. Tryptic peptides were identified using MS/MS analysis, which detected peptides covering 94% of the expected protein sequence, with only a small peptide C-terminal peptide containing Cys130 eluding observation. This data revealed the covalent modification of galectin-1 at five cysteine residues (Cys2, Cys16, Cys42, Cys60, Cys88) by **AuP1** in a manner consistent with C-S arylation, as indicated by the mass change $m/z = 181$ Da (Figure 9b-e). No modifications were observed on any of the other amino acid residues in the protein. This shows the chemoselectivity of Au(III) complexes toward the cysteine residues. Further, pull-down studies using MDA-MB-231 lysate unveiled galectin-1 enrichment based on immunoblotting. Covalent molecular modeling further revealed the interaction of the arylpyridine of **AuP1** interacting with hydrophobic side chains of the intrinsically disordered galectin-1 protein. Taken together, these studies provide evidence for covalent modification of IDPs via S-arylation of targetable cysteines.

Distinct Site Selectivity by AuP Versus Iodoacetamide (IAA) Using Time-Resolved Top-Down Proteomics

Time-resolved intact mass and top-down proteomics (Figures S64–S68) show that **AuP1** labeling is rapid, extensive, and site-specific, while iodoacetamide (IAA) is slow and highly restricted toward cysteines in solvent-exposed regions. **AuP1** efficiently modifies cysteines in disordered regions and buried regions of Galectin-1 (Cys42, Cys60, Cys88) within minutes and labels all six cysteines by 30 min, with Cys130 (the most solvent-exposed thiol) being the least reactive (Figure 10a,b). This generates a rich set of multi-modified proteoforms assessed by top-down proteoform counts (Figure 10c). In contrast, IAA modifies almost exclusively Cys130, the most solvent-exposed thiol, even after 2 h of incubation time, leaving other cysteines unmodified (Figure 10d–f) Thus, **AuP1** uniquely accesses both buried and disordered sites, providing a much broader picture of cysteine reactivity than conventional alkylation of IAA.

Conclusion

In this work, we developed and characterized a new class of [C^N]-cyclometalated Au(III)–monodentate phosphine complexes (**AuP1–AuP8**) to introduce a novel cysteine labeling platform combined with moderately rapid kinetics ($k_2 \approx 10^2$ M^{-1} s^{-1}) with a uniquely tunable steric shield that drives selectivity into hydrophobic IDR microenvironment thiols in proteins. This balance enables the first systematic targeting of "undruggable" intermediate-buried cysteines in IDRs with high occupancy (>64% at low micromolar concentrations) while minimizing off-target labeling in structured domains. These new benchmarks proved that, although faster arylation reagents exist, none achieve the critical "speed + IDP-selectivity" profile required for covalent proteome mapping of intrinsically disordered proteins.

This platform overcomes the long-standing limitations of conventional cysteine labeling probes' irreversible off-target reactivity, reversible covalent bonds, and affinity towards easily accessible and solvent-exposed sites to open entirely new frontiers in covalent chemical biology. Importantly, our work transforms intrinsically disordered regions, once considered beyond reach, into tractable therapeutic targets and lays the foundation for next-generation covalent drug discovery against proteins and interaction motifs that have eluded medicinal chemistry for decades.

Through an iterative design process, we synthesized Au(III)-aryl reagents with diverse phosphine ligands and demonstrated their ability to rapidly arylate cysteine in peptides and proteins. Kinetic analyses revealed how the steric bulk of phosphine ligands influences reaction rates, providing useful design principles for tuning the reactivity of future cysteine-targeting probes. Our findings demonstrate, for the first time, the selective targeting of cysteine residues within intrinsically disordered proteins and regions—overcoming a longstanding challenge in chemical biology. By integrating structural data, computational modeling, and chemoproteomic profiling, we showed that these Au(III) complexes exhibit tunable reactivity, fast kinetics, and broad proteome coverage. They are capable of labeling both conserved "hotspot" cysteines and transient, otherwise cryptic cysteine sites that have eluded conventional probes. Importantly, this Au(III)-mediated arylation platform significantly expands the accessible cysteinome and opens new avenues for covalent drug discovery, particularly against IDPs and other challenging protein classes implicated in disease. For example, the successful labeling of galectin-1 and numerous other previously unliganded targets underscores the potential of **AuP** complexes as versatile tools for biological investigation and therapeutic development. Overall, our work establishes a foundation for exploring metal-based covalent modifiers as next-generation probes, and it highlights the promise of chemoproteomic strategies in advancing the targeting of the human proteome's most elusive regions.

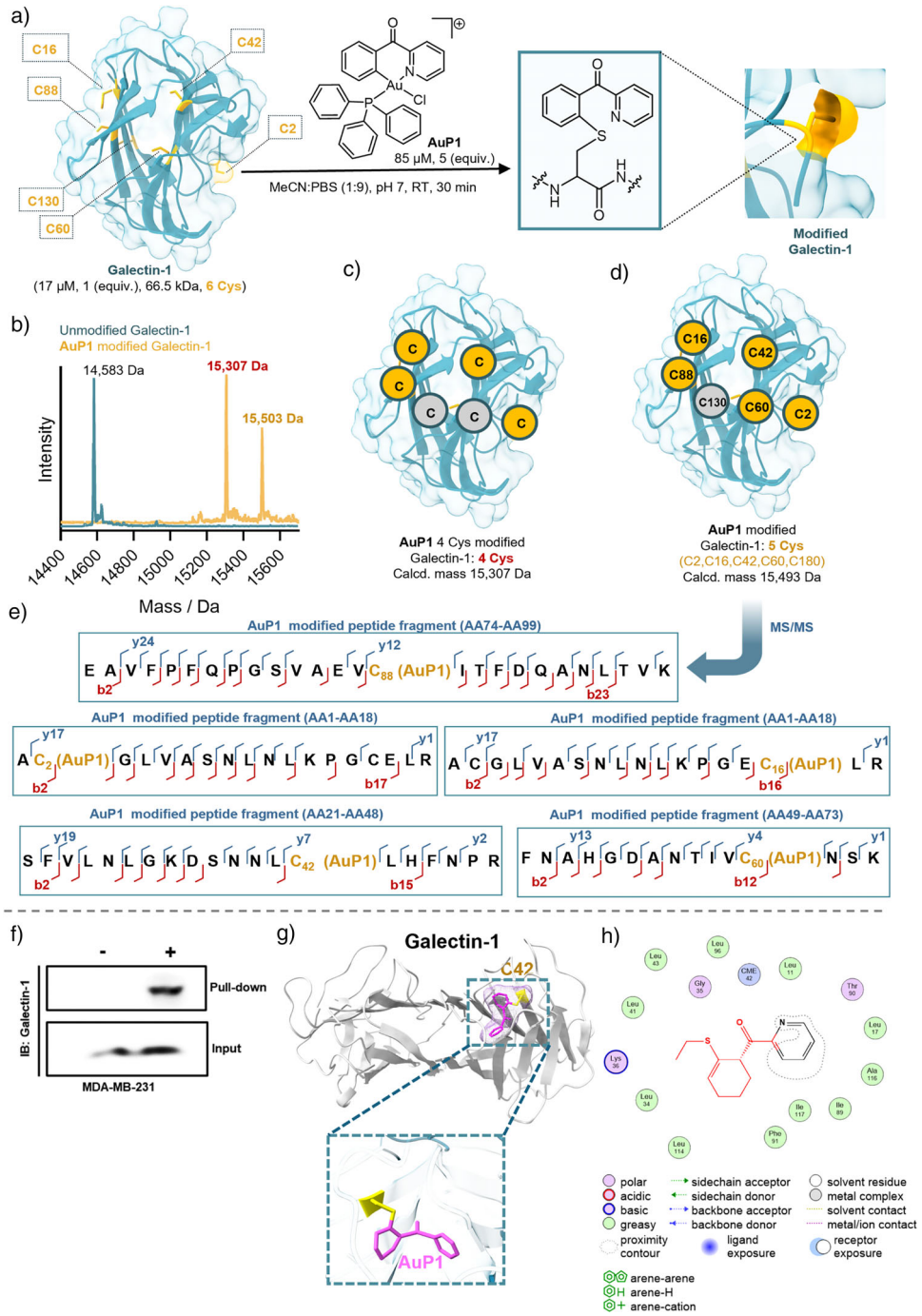

Figure 9. Cysteine-specific protein modification. a) Reaction conditions: **AuP1** (86.2 µM) was incubated with Galectin-1 (17.2 µM) at rt in PBS buffer with a pH of 7.4 (protein: Au(III) complex = 1:5). b) Deconvoluted LC/MS spectrum shows site-specific protein modification with **AuP1**, where it modified *5* cysteines in Galectin-1. c) **AuP1** modified 4 cysteines. d) **AuP1** modified 5 cysteines. e) The tryptic peptides formed from Galectin-1 and **AuP1**, confirming Cys88, Cys2, Cys16, Cys42, and Cys60 modifications. f) Immunoblotting of pull-down validation of LGALS1 as the target of AuP1. The input blot is indicative of the amount of LGALS1 in the lysates. g) Illustration and molecular docking of Au(III)-mediated cysteine arylation: Structural model and computational docking depict the covalent arylation of Cys42 residue by cyclometalated Au(III) complex bearing a monodentate phosphine ligand, **AuP1** (PDB: 1GZW). h) 2-D Protein–ligand interaction of **AuP1** and galectin-1. This figure highlights, for the first time, the predicted binding orientation and reaction mechanism at the cysteine site, providing structural insight into gold-mediated bioconjugation with protein targets.

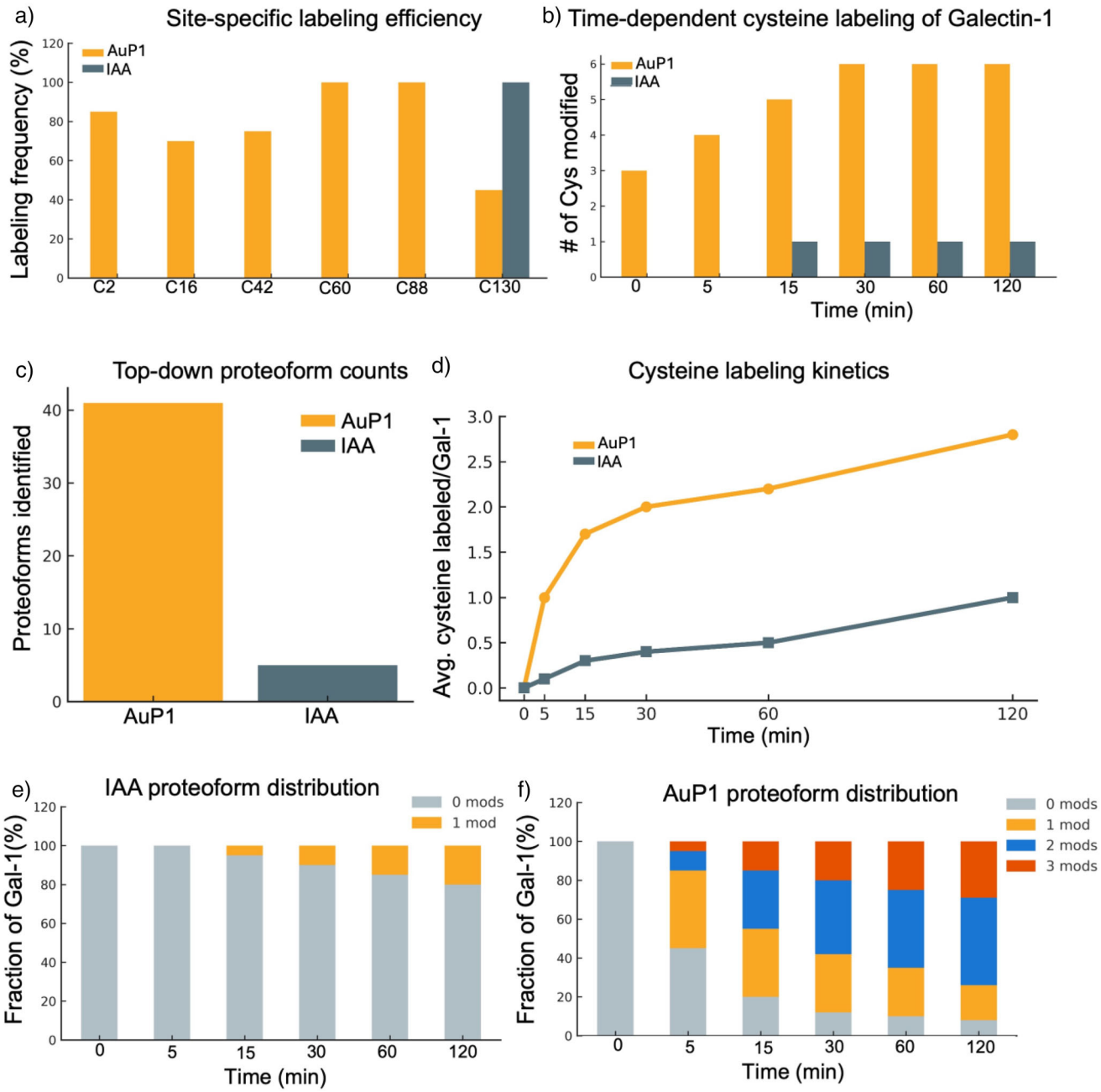

Figure 10. a) Labeling frequency and efficiency of galectin-1 (20 μM) by IAA or **AuP1** (protein: IAA or Au(III) complex, **AuP1** (100 μM) = 1:5) at room temperature in PBS buffer with a pH of 7.4. b) Cysteine-specific galectin-1 modification in a time-dependent manner over 2 h. Reactions were quenched with cysteine (100 mM) at each time point and placed on ice prior to LC-MS/MS workflows. c) Top-down proteoform count analysis by **AuP1**- or IAA-induced galectin modification. d) Analysis of average cysteine labeled by IAA or **AuP1** per galectin molecule over time. e) IAA proteoform distribution over time; mainly single cysteine modified galectin-1 species are detected with minimal change over time. f) **AuP1** proteoform distribution over time; the most abundant 1 to 3 cysteines-modified galectin-1 species are shown; low-abundance 4 to 6 cysteine-modified galectin-1 species were omitted for clarity.

Supporting Information

Details about instruments, materials, methods, chemical synthesis, ^{1}H and ^{31}P NMR characterization, stopped flow data, LC-MS characterization, computational information, and proteomics data. CCDC 2372388, 2372389, 2372390, 2372391, and 2372392 contain the supplementary crystallographic data for this paper. These data can be obtained free of charge via www.ccdc.cam.ac.uk/data_request/cif, or by emailing data_request@ccdc.cam.ac.uk, or by contacting The Cambridge Crystallographic Data Centre, 12 Union Road, Cambridge CB2 1EZ, UK.

Author Contributions

Udara Munugoda: Conceptualization; methodology; synthesis and characterization; python coding; data generation; data analyzing; interpretation related to Proteomics data base comparison study; writing original; draft preparation; writing, review and editing. **Sean T. Gilpatrick**: Python coding; data generation; data analyzing; interpretation related to Proteomics data base comparison study; writing, review and editing. **Debarati Das**: Stopped flow kinetics; writing, review and editing. **Sean Parkin**: X-ray crystallography; writing, review and editing. **Anne-Frances Miller**: Stopped flow kinetics; writing, review and editing. **Samuel G. Awuah**: Conceptualization; methodology; python coding; data generation; data analyzing; interpretation related to Proteomics data base comparison study; writing original; draft preparation; supervision; funding acquisition; writing, review and editing.

Acknowledgements

This research was funded by the National Science Foundation's Chemistry of Life Processes program (Award CHE-2203559) for S.G.A. D.D. was supported by NSF award CHE 2108134 to A.-F.M. S.G.A is also supported by R01CA258421 from the National Cancer Institute. The authors used the MOE 2022.02 version for molecular docking studies, which was supported by NCI Cancer Center Support Grant (P30 CA177558). The authors gratefully acknowledge the support of various facilities at the University of Kentucky, including the UK NMR Center (NSF-CHE-997738) and the UK X-ray facility (NSF-CHE-1625732). The authors also appreciate the assistance of Dr. Andrew Lemoff and the Proteomics Core facility at UT Southwestern for mass spectrometry and proteomics expertise. The authors acknowledge Awuah group members Chibuzor Olelewe and Oluwatosin Obisesan for experimental assistance. Thanks to Sashen Ruhunage for assistance in computational analysis.

Conflict of Interests

The authors declare the following financial interests/personal relationships, which may be considered as potential competing interests: Samuel G. Awuah has patents pending to the University of Kentucky Research Foundation.

Data Availability Statement

The data that support the findings of this study are available from the corresponding author upon reasonable request.

Keywords: Bioorthogonal chemistry · Covalent modification · Cysteine arylation · Gold(III) complexes · Intrinsically disordered proteins (IDPs) · Protein bioconjugation · Proteomics

[1] K. K. Kung, H. M. Ko, J. F. Cui, H. C. Chong, Y. C. Leung, M. K. Wong, *Chem. Commun.* **2014**, *50*, 11899–11902, https://doi.org/10.1039/C4CC04467C.
[2] S. Gukathasan, S. Parkin, E. P. Black, S. G. Awuah, *Inorg. Chem.* **2021**, *60*, 14582–14593, https://doi.org/10.1021/acs.inorgchem.1c01517.
[3] M. S. Messina, J. M. Stauber, M. A. Waddington, A. L. Rheingold, H. D. Maynard, A. M. Spokoyny, *J. Am. Chem. Soc.* **2018**, *140*, 7065–7069, https://doi.org/10.1021/jacs.8b04115.
[4] C. D. Spicer, B. G. Davis, *Nat. Commun.* **2014**, *5*, 4740, https://doi.org/10.1038/ncomms5740.
[5] A. Beck, L. Goetsch, C. Dumontet, N. Corvaïa, *Nat. Rev. Drug Discovery* **2017**, *16*, 315–337, https://doi.org/10.1038/nrd.2016.268.
[6] S. Lin, X. Yang, S. Jia, A. M. Weeks, M. Hornsby, P. S. Lee, R. V. Nichiporuk, A. T. Iavarone, J. A. Wells, F. D. Toste, *Science* **2017**, *355*, 597.
[7] H. Seki, S. J. Walsh, J. D. Bargh, J. S. Parker, J. Carroll, D. R. Spring, *Chem. Sci.* **2021**, *12*, 9060.
[8] R. Frei, J. Waser, *J. Am. Chem. Soc.* **2013**, *135*, 9620.
[9] F. J. Chen, J. Gao, *Chem.–Euro. J.* **2022**, *28*, e202201843.
[10] E. A. Doud, J. A. Tilden, J. W. Treacy, E. Y. Chao, H. R. Montgomery, G. E. Kunkel, E. J. Olivares, N. Adhami, T. A. Kerr, Y. Chen, *J. Am. Chem. Soc.* **2024**, *146*, 12365.
[11] Y. Tian, and Q. Lin, *Chem. Biol.* **2019**, *14*, 2489–2496. https://doi.org/10.1021/acschembio.9b00755.
[12] F. J. Chen, M. Zheng, V. Nobile, J. Gao, *Chem.–Euro. J.* **2022**, *28*, e202200058.
[13] J. M. Ravasco, H. Faustino, A. Trindade, P. M. Gois, *Chem.–Euro. J.* **2019**, *25*, 43–59, https://doi.org/10.1002/chem.201803174.
[14] E. A. Doud, J. A. Tilden, J. W. Treacy, E. Y. Chao, H. R. Montgomery, G. E. Kunkel, E. J. Olivares, N. Adhami, T. A. Kerr, Y. Chen, *J. Am. Chem. Soc.* **2024**, *26*, 10875–10879.
[15] P. Ochtrop, C. P. R. Hackenberger, *Curr. Opin. Chem. Biol.* **2020**, *58*, 28–36, https://doi.org/10.1016/j.cbpa.2020.04.017.
[16] E. A. Hoyt, P. M. Cal, B. L. Oliveira, G. J. Bernardes, *Nat. Rev. Chem.* **2019**, *3*, 147.
[17] R. P. Lyon, J. R. Setter, T. D. Bovee, S. O. Doronina, J. H. Hunter, M. E. Anderson, C. L. Balasubramanian, S. M. Duniho, C. I. Leiske, F.u Li, P. D. Senter, *Nat. Biotechnol.* **2014**, *32*, 1059–1062, https://doi.org/10.1038/nbt.2968.
[18] X. Chen, H. Wu, C.-M. Park, T. H. Poole, G. Keceli, N. O. Devarie-Baez, A. W. Tsang, W. T. Lowther, L. B. Poole, S. B. King, M. Xian, C. M. Furdui, *ACS Chem. Biol.* **2017**, *12*, 2201–2208, https://doi.org/10.1021/acschembio.7b00444.
[19] E. M. Allouche, E. Grinhagena, J. Waser, *Angew. Chem. Int. Ed.* **2022**, *61*, e202112287, https://doi.org/10.1002/anie.202112287.
[20] A. Istrate, M. B. Geeson, C. D. Navo, B. B. Sousa, M. C. Marques, R. J. Taylor, T. Journeaux, S. R. Oehler, M. R. Mortensen, M. J. Deery, A. D. Bond, F. Corzana, G. Jiménez-Osés, G. J. L. Bernardes, *J. Am. Chem. Soc.* **2022**, *144*, 10396–10406, https://doi.org/10.1021/jacs.2c02185.
[21] M. S. Messina, J. M. Stauber, M. A. Waddington, A. L. Rheingold, H. D. Maynard, A. M. Spokoyny, *J. Am. Chem. Soc.* **2018**, *140*, 7065.
[22] E. V. Vinogradova, C. Zhang, A. M. Spokoyny, B. L. Pentelute, S. L. Buchwald, *Nature* **2015**, *526*, 687–691, https://doi.org/10.1038/nature15739.
[23] X. Lin, E. Haimov, B. Redko, A. Vigalok, *Angew. Chem.* **2022**, *134*, e202205368.
[24] T. Schlatzer, J. Kriegesmann, H. Schröder, M. Trobe, C. Lembacher-Fadum, S. Santner, A. V. Kravchuk, C. F. Becker, R. Breinbauer, *J. Am. Chem. Soc.* **2019**, *141*, 14931.
[25] C. Zhang, E. V. Vinogradova, A. M. Spokoyny, S. L. Buchwald, B. L. Pentelute, *Angew. Chem. Int. Ed.* **2019**, *58*, 4810.

[26] M. N. Wenzel, R. Bonsignore, S. R. Thomas, D. Bourissou, G. Barone, A. Casini, *Chem.–Euro. J.* **2019**, *25*, 7628–7634, https://doi.org/10.1002/chem.201901535.
[27] H. R. Montgomery, M. S. Messina, E. A. Doud, A. M. Spokoyny, H. D. Maynard, *Bioconjugate Chem.* **2022**, *33*, 1536–1542, https://doi.org/10.1021/acs.bioconjchem.2c00280.
[28] J. A. R. Tilden, A. T. Lubben, S. B. Reeksting, G. Kociok-Köhn, C. G. Frost, *Chem.–Euro. J.* **2022**, *28*, e202104385, https://doi.org/10.1002/chem.202104385.
[29] R. T. Mertens, S. Gukathasan, A. S. Arojojoye, C. Olelewe, S. G. Awuah, *Chem. Rev.* **2023**, *123*, 6612–6667, https://doi.org/10.1021/acs.chemrev.2c00649.
[30] M. Mora, M. C. Gimeno, R. Visbal, *Chem. Soc. Rev.* **2019**, *48*, 447–462, https://doi.org/10.1039/C8CS00570B.
[31] S. Yue, M. Luo, H. Liu, S. Wei, *Front. Chem.* **2020**, *8*, 543, https://doi.org/10.3389/fchem.2020.00543.
[32] A. S. Arojojoye, B. Walker, J. C. Dawahare, M. A. O. Afrifa, S. Parkin, S. G. Awuah, *ACS Appl. Mater. Interfaces* **2023**, *15*, 43607–43620, https://doi.org/10.1021/acsami.3c10025.
[33] S. Gukathasan, O. A. Obisesan, S. Saryazdi, L. Ratliff, S. Parkin, R. B. Grossman, S. G. Awuah, *Inorg. Chem.* **2023**, *62*, 13118–13129, https://doi.org/10.1021/acs.inorgchem.3c02066.
[34] S. Gukathasan, S. Parkin, E. P. Black, S. G. Awuah, *Inorg. Chem.* **2021**, *60*, 14582.
[35] C. Olelewe, J. H. Kim, S. Ofori, R. T. Mertens, S. Gukathasan, S. G. Awuah, *Iscience* **2022**, *25*, 104340, https://doi.org/10.1016/j.isci.2022.104340.
[36] R. T. Mertens, C. E. Greif, J. T. Coogle, G. Berger, S. Parkin, M. D. Watson, S. G. Awuah, *J. Catal.* **2022**, *408*, 109–114, https://doi.org/10.1016/j.jcat.2022.02.019.
[37] S. Ofori, S. Gukathasan, S. G. Awuah, *Chem.–Euro. J.* **2021**, *27*, 4168–4175, https://doi.org/10.1002/chem.202004962.
[38] J. N. Spradlin, E. Zhang, D. K. Nomura, *Acc. Chem. Res.* **2021**, *54*, 1801–1813, https://doi.org/10.1021/acs.accounts.1c00065.
[39] S. Moon, B.-H. Lee, *Mol. Cells* **2018**, *41*, 933.
[40] W. F. An, N. Tolliday, *Mol. Biotechnol.* **2010**, *45*, 180–186, https://doi.org/10.1007/s12033-010-9251-z.
[41] W. Lu, M. Kostic, T. Zhang, J. Che, M. P. Patricelli, L. H. Jones, E. T. Chouchani, N. S. Gray, *RSC Chem. Biol.* **2021**, *2*, 354–367, https://doi.org/10.1039/D0CB00222D.
[42] G. Drewes, S. Knapp, *Trends Biotechnol.* **2018**, *36*, 1275–1286, https://doi.org/10.1016/j.tibtech.2018.06.008.
[43] A. Cuesta, J. Taunton, *Annu. Rev. Biochem.* **2019**, *88*, 365–381, https://doi.org/10.1146/annurev-biochem-061516-044805.
[44] R. J. Grams, K.-L. Hsu, *Trends Pharmacol. Sci.* **2022**, *43*, 249–262, https://doi.org/10.1016/j.tips.2021.12.002.
[45] J. S. Fetrow, N. Siew, J. Skolnick, *FASEB J.* **1999**, *13*, 1866–1874, https://doi.org/10.1096/fasebj.13.13.1866.
[46] I. M. Serafimova, M. A. Pufall, S. Krishnan, K. Duda, M. S. Cohen, R. L. Maglathlin, J. M. McFarland, R. M. Miller, M. Frödin, J. Taunton, *Nat. Chem. Biol.* **2012**, *8*, 471.
[47] L. Huang, Z. Guo, F. Wang, L. Fu, *Signal Transduct. Tar.* **2021**, *6*, 386.
[48] E. Leproult, S. Barluenga, D. Moras, J.-M. Wurtz, N. Winssinger, *J. Med. Chem.* **2011**, *54*, 1347–1355, https://doi.org/10.1021/jm101396q.
[49] G. Erdős, B. Mészáros, D. Reichmann, Z. Dosztányi, *Proteomics* **2019**, *19*, 1800070, https://doi.org/10.1002/pmic.201800070.
[50] E. Shanina, S. Kuhaudomlarp, E. Siebs, F. F. Fuchsberger, M. Denis, P. da Silva Figueiredo Celestino Gomes, M. H. Clausen, P. H. Seeberger, D. Rognan, A. Titz, *Commun. Chem.* **2022**, *5*, 64.
[51] L. Boike, A. G. Cioffi, F. C. Majewski, N. J. Henning, M. D. Jones, G. Liu, J. M. McKenna, J. A. Tallarico, M. Schirle, D. K. Nomura, *Cell Chem. Biol.* **2021**, *28*, 4.
[52] Z.-Z. Wang, X.-X. Shi, G.-Y. Huang, G.-F. Hao, G.-F. Yang, *Trends Biochem. Sci.* **2023**, *48*, 539–552, https://doi.org/10.1016/j.tibs.2023.01.008.
[53] W. A. Munzeiwa, B. Omondi, V. O. Nyamori, *Beilstein J. Org. Chem.* **2020**, *16*, 362–383, https://doi.org/10.3762/bjoc.16.35.
[54] P. D. Lyne, D. M. P. Mingos, *J. Organomet. Chem.* **1994**, *478*, 141–151, https://doi.org/10.1016/0022-328X(94)88166-9.
[55] E. A. Doud, J. A. Tilden, J. W. Treacy, E. Y. Chao, H. R. Montgomery, G. E. Kunkel, E. J. Olivares, N. Adhami, T. A. Kerr, Y. Chen, *J. Am. Chem. Soc.* **2024**, *146*, 12365–12374.
[56] K. K.-Y. Kung, H.-M. Ko, J.-F. Cui, H.-C. Chong, Y.-C. Leung, M.-K. Wong, *Chem. Commun.* **2014**, *50*, 11899–11902, https://doi.org/10.1039/C4CC04467C.
[57] R. E. F. De Paiva, Z. Du, D. H. Nakahata, F. A. Lima, P. P. Corbi, N. P. Farrell, *Angew. Chem. Int. Ed.* **2018**, *57*, 9305–9309, https://doi.org/10.1002/anie.201803082.
[58] K. Li, J. Xia, M. A. Mehmood, X.-Q. Zhao, C.-G. Liu, F.-W. Bai, *Chem. Eng. Sci.* **2019**, *196*, 54–63, https://doi.org/10.1016/j.ces.2018.11.059.
[59] J. W. Treacy, J. A. R. Tilden, E. Y. Chao, Z. Fu, A. M. Spokoyny, K. N. Houk, H. D. Maynard, *Chem. Sci.* **2025**, *16*, 3878–3887, https://doi.org/10.1039/D4SC05920D.
[60] L. Falivene, Z. Cao, A. Petta, L. Serra, A. Poater, R. Oliva, V. Scarano, L. Cavallo, *Nat. Chem.* **2019**, *11*, 872–879, https://doi.org/10.1038/s41557-019-0319-5.
[61] Gaussian 16, Revision A.03, M. J. Frisch, G. W. Trucks, H. B. Schlegel, G. E. Scuse-ria, M. A. Robb, J. R. Cheeseman, G. Scalmani, V. Barone, G. A. Peters-son, H. Nakatsuji, X. Li, M. Caricato, A. V. Marenich, J. Bloino, B. G. Janesko, R. Gomperts, B. Mennucci, H. P. Hratchian, J. V. Ortiz, A. F. Izmaylov, J. L. Sonnenberg, D. Williams-Young, F. Ding, F. Lipparini, F. Egidi, J. Goings, B. Peng, A. Petrone, T. Henderson, D. Ranasinghe, et al., Gaussian, Inc., Wallingford CT, **2016**.
[62] A. V. Marenich, C. J. Cramer, D. G. Truhlar, *J. Phys. Chem. B* **2009**, *113*, 6378–6396, https://doi.org/10.1021/jp810292n.
[63] J.-D. Chai, M. Head-Gordon, *Phys. Chem. Chem. Phys.* **2008**, *10*, 6615, https://doi.org/10.1039/b810189b.
[64] F. Weigend, R. Ahlrichs, *Phys. Chem. Chem. Phys.* **2005**, *7*, 3297, https://doi.org/10.1039/b508541a.
[65] F. Weigend, *Phys. Chem. Chem. Phys.* **2006**, *8*, 1057, https://doi.org/10.1039/b515623h.
[66] K. M. Backus, B. E. Correia, K. M. Lum, S. Forli, B. D. Horning, G. E. González-Páez, S. Chatterjee, B. R. Lanning, J. R. Teijaro, A. J. Olson, D. W. Wolan, B. F. Cravatt, *Nature* **2016**, *534*, 570–574, https://doi.org/10.1038/nature18002.
[67] M. E. H. White, J. Gil, and E. W. Tate, *Cell Chem. Biol.* **2023**, 828–838.e4. https://doi.org/10.1016/j.chembiol.2023.06.021.
[68] L. Skos, C. Schmidt, S. R. Thomas, M. Park, V. Geiger, D. Wenisch, R. Bonsignore, G. Del Favero, T. Mohr, A. Bileck, C. Gerner, A. Casini, S. M. Meier-Menches, *Cell Rep. Phys. Sci.* **2024**, *5*, 102072, https://doi.org/10.1016/j.xcrp.2024.102072.
[69] M. Chetry, Y. Song, C. Pan, R. Li, J. Zhang, X. Zhu, *J. Cancer* **2020**, *11*, 1584–1595, https://doi.org/10.7150/jca.38538.
[70] M. B. Sauerland, C. Helm, L. G. Lorentzen, A. Manandhar, T. Ulven, L. F. Gamon, M. J. Davies, *Redox Biol.* **2023**, *59*, 102560, https://doi.org/10.1016/j.redox.2022.102560.

Manuscript received: July 25, 2025
Revised manuscript received: September 29, 2025
Manuscript accepted: October 06, 2025
Version of record online: ■■, ■■